processes

MDPI

Article

Integrated Assessment of Solid, Liquid, and Gaseous Fuels Derived from Fixed-Bed Pyrolysis of Waste Tires

Harryson Guimarães de Lima [1], Clériston Moura Vieira Júnior [2], Humberto Santos [3], Adalberto Freire do Nascimento Júnior [1], Antônio Celso Dantas Antonino [2,*] and Sérgio Peres Ramos da Silva [1]

[1] Fuel and Energy Laboratory, Mechanical Engineering Department, Polytechnic School of Pernambuco, University of Pernambuco, Recife 50720-001, Brazil; adalbertofreire2@gmail.com (A.F.d.N.J.); sergio.peres@upe.br (S.P.R.d.S.)
[2] Department of Nuclear Energy, Federal University of Pernambuco, Recife 50670-901, Brazil; cleriston.vieira@ufpe.br
[3] Thermal Engineering and Energy Systems Group, Aragón Institute for Engineering Research (I3A), University of Zaragoza, Agustín de Betancourt Buildinng, C/Maria de Luna 3, 50018 Zaragoza, Spain; hdasilva@unizar.es
* Correspondence: antonio.antonino@ufpe.br

Abstract

The improper disposal of end-of-life tires poses significant environmental challenges due to their petroleum-based composition and slow degradation, while simultaneously representing an underutilized energy resource. This study investigates the slow pyrolysis of shredded waste tires in a fixed-bed electrically heated reactor to evaluate the production and fuel properties of gaseous, liquid, and solid fractions. Experiments were conducted with 100 g samples under nitrogen at final temperatures of 400, 500, and 600 °C, with residence times of 40, 25, and 10 min, respectively. Higher temperatures promoted gas formation, increasing yields from 27% to 32% and achieving a maximum lower heating value of 30.54 MJ m^{-3} at 600 °C, with enhanced H_2 and CH_4 contents. Solid yields decreased slightly (41% to 37%), while char maintained stable heating values (~29 MJ kg^{-1}). Liquid yields remained near 33% and showed high calorific values (~41 MJ kg^{-1}), densities of 700–770 kg m^{-3}, low acidity, low ash content, and increased viscosity at higher temperatures. Energy conversion efficiency reached 74.4% at 500 °C. The integrated evaluation of all fractions under identical conditions highlights fixed-bed pyrolysis as a promising pathway for waste-tire valorization and decentralized fuel production.

Keywords: waste tires; slow pyrolysis; fixed-bed reactor; liquid fuels; gaseous fuels; solid fuel; thermochemical conversion

Academic Editors: Xin Yao and Huaqing Xie

Received: 20 February 2026
Revised: 18 March 2026
Accepted: 3 April 2026
Published: 9 April 2026

1. Introduction

The continuous growth of the global vehicle fleet, together with urban expansion and industrial development, has led to a steady increase in the generation of end-of-life tires, which represent one of the most challenging solid waste streams from both environmental and technological perspectives. Due to their complex composition, high durability, and resistance to natural degradation, waste tires pose significant environmental and public health risks when improperly managed. At the same time, they constitute an important secondary resource, rich in carbonaceous and energetic compounds, motivating increasing research interest in sustainable valorization routes consistent with circular economy principles [1,2].

From an energy perspective, waste tires exhibit high calorific values comparable to those of conventional fossil fuels, owing to their high content of natural and synthetic rubbers, carbon black, and hydrocarbon additives. Among the available treatment technologies, pyrolysis has been widely recognized as a promising thermochemical route for tire valorization, enabling the conversion of polymeric materials under oxygen-free conditions into three main product fractions: a solid carbon-rich char, a liquid oil dominated by hydrocarbons, and a non-condensable combustible gas mixture [1,3,4]. This intrinsic versatility has positioned tire pyrolysis as a flexible platform for both energy recovery and material recycling.

Extensive experimental and review studies have demonstrated that product distribution and quality in waste tire pyrolysis are strongly dependent on operational parameters, including final temperature, heating rate, residence time, and reactor configuration [1,3–5]. In particular, the liquid fraction has received considerable attention due to its relatively high heating value and the presence of valuable compounds, including limonene and mono-aromatic hydrocarbons [6–8]. Consequently, several studies have investigated the direct use of tire pyrolysis oil as a fuel, as well as its upgrading and co-processing with petroleum-derived streams [9–11].

Despite these advances, the literature remains largely fragmented. A significant number of studies focus predominantly on a single product fraction, most commonly the liquid oil, while treating the solid char and gaseous products as secondary outputs. Other works address the utilization of char as a solid fuel, adsorbent, catalyst precursor, or reinforcing filler, or analyze the gas fraction with emphasis on heat, power generation, or hydrogen recovery [12–15]. This compartmentalized approach limits the establishment of consistent mass and energy balances and hampers a holistic assessment of the overall performance of the pyrolysis process.

From a technological standpoint, a wide variety of reactor concepts have been investigated for waste tire pyrolysis, including fixed-bed, fluidized-bed, rotary kiln, tubular, microwave-assisted, plasma-based, and molten-salt-heated systems [3–5,16–18]. Advanced configurations, such as microwave and molten-salt heating, have been reported to enhance heat transfer and temperature uniformity. However, they also introduce additional challenges related to system complexity and scalability [4,17]. Nevertheless, fixed-bed reactors remain relevant due to their simplicity, robustness, and suitability for laboratory-scale investigations and decentralized applications, particularly in early-stage process evaluation.

Another critical issue associated with waste tire pyrolysis concerns the presence and behavior of sulfur, which originates mainly from vulcanization additives used in tire manufacturing. Sulfur distribution among oil, gas, and char fractions directly affects fuel quality, emissions, and downstream utilization. Recent studies have explored sulfur migration and transformation mechanisms during pyrolysis, as well as in situ and ex situ strategies for sulfur fixation or removal using catalysts or alternative heating methods [19,20]. Despite these efforts, effective sulfur control remains a major technological challenge.

Beyond energy recovery, increasing attention has been directed toward the chemical valorization of tire pyrolysis products. Pyrolysis oils can serve as feedstocks for the production of higher-value chemicals through catalytic upgrading and other transformation routes, highlighting the potential of waste tire pyrolysis as a source of valuable chemical compounds in addition to fuels and solid materials [7,21,22]. These developments further reinforce the need to consider waste tire pyrolysis as an integrated conversion process rather than a single-objective waste treatment technology.

From a mechanistic and kinetic perspective, recent studies employing thermogravimetric analysis, Py-GC/MS, and kinetic modeling have contributed to a deeper understanding

of decomposition pathways and product formation during tire pyrolysis, highlighting the influence of rubber composition and operating conditions on reaction mechanisms [22,23]. However, many of these investigations are conducted under analytical or micro-scale conditions, limiting their direct applicability to conventional laboratory or pilot-scale reactors.

In this context, there remains a clear need for studies that provide an integrated evaluation of the solid, liquid, and gaseous products generated from waste tire pyrolysis under identical and well-controlled experimental conditions. Such an approach is essential for establishing reliable mass and energy balances, assessing overall energetic performance, and identifying realistic opportunities for internal energy integration.

Accordingly, the objective of this study is to investigate the slow pyrolysis of waste tires in a batch-operated fixed-bed reactor under an inert nitrogen atmosphere at different final temperatures. The waste tires are collected in the state of Pernambuco, Brazil. Unlike many previous studies, this work presents a comprehensive and integrated characterization of the solid char, liquid oil, and non-condensable gas fractions obtained from the same experimental runs, with particular emphasis on their energetic properties. The results aim to contribute to a more holistic understanding of waste tire pyrolysis as a sustainable route for resource and energy recovery.

2. Materials and Methods

2.1. Characterization and Preparation of the Feedstock

2.1.1. Origin, Cleaning, and Fragmentation of Rubber

The feedstock used in this study consisted of end-of-life passenger car tires obtained from different manufacturers, aiming to ensure a representative composition of the rubber typically available in the Brazilian urban environment. The waste tires used to compose the samples were collected in Pernambuco, Brazil. Initially, all tire units were subjected to a manual cleaning procedure to remove adhered impurities, thereby ensuring quality control and reproducibility in subsequent analyses.

The mechanical separation of the rubber from the metallic reinforcements was carried out using appropriate tools. The sidewall rubber was sectioned into chips with approximate dimensions of 80 × 40 × 10 mm using industrial cutting knives, ensuring comparable geometries among samples. The tread rubber, in turn, was extracted using a bench drill equipped with deliberately blunted wood drill bits. This strategy enabled the removal of the rubber without inducing significant heating, thereby minimizing the risk of premature thermal degradation. As a result, the process generated heterogeneous fragments with irregular particle sizes, a characteristic inherent to the extraction method employed.

2.1.2. Homogenization and Sample Preparation

In order to ensure that each pyrolysis run adequately represented the overall tire composition, the sidewall and tread rubber fractions were initially separated according to manufacturer. The mass proportion between these two components was then determined using a digital analytical balance with a resolution of four decimal places. For each experimental run, samples with a total mass of 100 g were prepared based on this previously established mass ratio, ensuring both homogeneity and representativeness.

All available tire brands were included in each sample, thereby eliminating compositional biases associated with individual manufacturers and enhancing the robustness and general applicability of the experimental results.

2.2. Thermal and Calorimetric Characterization

2.2.1. Thermogravimetric Analysis (TGA)

The initial thermal characterization was performed using a Shimadzu DTG-60 thermogravimetric analyzer. The sample was carefully distributed within the crucible, completely filling its volume in order to ensure adequate thermal contact. The heating was conducted at a controlled rate of 10 °C·min^{-1} up to a final temperature of 900 °C, which is sufficient to promote complete degradation of the rubber matrix followed by the combustion of fixed carbon.

Once the temperature stabilized at the final setpoint, oxygen (O_2) was injected into the system, triggering the oxidation of the remaining carbon and allowing its indirect quantification. Based on the mass loss data obtained throughout the analysis, the contents of moisture, volatile matter, and ash were determined, while the fixed carbon content was calculated according to ASTM D3172–89 [24]. This analysis provided essential insights into the thermal behavior of the rubber feedstock and supported the selection of the operational temperatures adopted in the pyrolysis experiments.

2.2.2. Calorimetric Analysis of Rubber and Pyrolysis Fuels

The higher heating value (HHV) and lower heating value (LHV) of the rubber feedstock, as well as those of the liquid and solid products obtained from pyrolysis, were determined in accordance with ABNT NBR 8633:1984 [25] using a digital bomb calorimeter (Ika-Werke C2000 Control). Sample masses ranging from 0.3 to 0.5 g were weighed into previously cleaned and dried crucibles to ensure analytical accuracy.

For the determination of the LHV, the calorimetric procedure was complemented by successive titrations using standardized sodium hydroxide (NaOH) and hydrochloric acid (HCl) solutions after washing the combustion vessel with 50 mL of distilled water. This procedure enabled quantification of the mass of water formed during combustion, a critical parameter for accurate LHV calculation.

2.3. Pyrolysis System and Operating Conditions

2.3.1. Reactor Description and Main Components

The pyrolysis experiments were carried out in a batch-operated fixed-bed reactor originally designed and manufactured in the previous work [26]. The reactor was constructed from seamless AISI 304 stainless steel (Schedule 40S), selected for its high mechanical strength and resistance to corrosion at elevated temperatures. The reactor presented an internal diameter of 62.71 mm, a total height of 260 mm, and a wall thickness of 5.16 mm.

Heating was provided by electrical resistance elements with a total installed power of 3000 W, uniformly distributed around the reactor body to promote homogeneous heat transfer. The heating system was thermally insulated using a fiberglass blanket to minimize heat losses and enhance temperature stability during operation. Reactor temperature was monitored and controlled by a type-K thermocouple installed at the top of the reactor and connected to a digital temperature controller, ensuring accurate regulation of the operating conditions throughout the experimental runs.

The reactor was operated in batch mode and was capable of reaching temperatures of up to 700 °C, with controllable heating rates ranging from 1 to 20 °C·min^{-1}. Nitrogen (N_2) was used as an inert carrier gas and introduced through the lower inlet of the reactor. The gas flow rate was regulated by a pressure regulator and a rotameter installed downstream of the nitrogen cylinder. The gaseous products exited the reactor through the upper outlet and were subsequently directed to the condensation and gas-cleaning units.

All connections within the pyrolysis system were made using flexible silicone tubing with an internal diameter of 2 mm and an external diameter of 5 mm, ensuring gas-tight

operation and ease of assembly. Nitrogen was selected as the carrier gas due to its low cost and availability when compared to other inert gases, such as argon.

Figure 1 schematically illustrates the complete experimental pyrolysis system employed in this study. The setup consists of (1) a nitrogen (N_2) gas cylinder supplying the inert atmosphere, (2) a fixed-bed reactor where the pyrolysis reactions take place, (3) a condenser responsible for cooling and condensing the volatile products, (4) a gas filtration unit for the removal of particulates and condensable residues, (5) a gas sampling bag used for collecting the non-condensable gaseous products, and (6) a rotameter installed in the outlet gas line to control and monitor the gas flow rate.

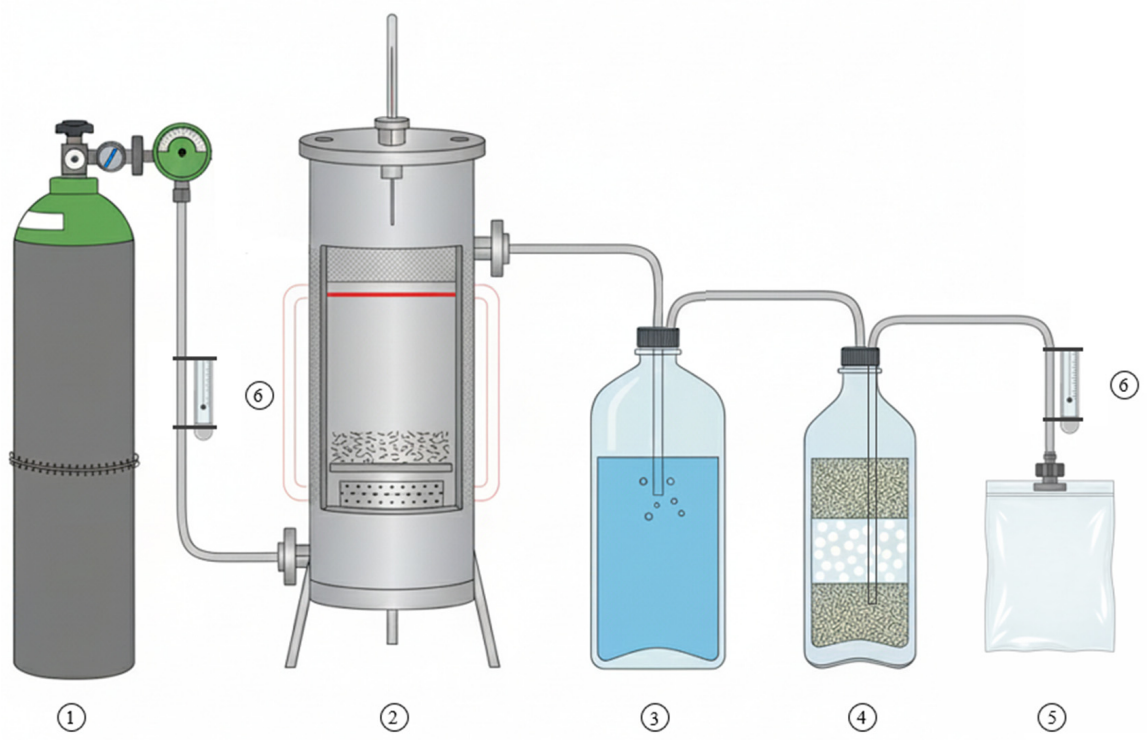

Figure 1. Schematic illustration of the complete pyrolysis system employed in this study. The components of the setup are: (1) nitrogen (N_2) gas cylinder supplying the inert atmosphere, (2) fixed-bed reactor where the pyrolysis reactions take place, (3) condenser responsible for cooling and condensing the volatile products, (4) gas filtration unit for the removal of particulates and condensable residues, (5) gas sampling bag used for collecting the non-condensable gaseous products, and (6) rotameter installed in the outlet gas line to control and monitor the gas flow rate.

In the experimental setup, the condenser illustrated as item (3) in Figure 1 operates as a bubble-type condenser. The pyrolysis vapors leaving the reactor are introduced into a water-filled glass bottle and forced to bubble through the liquid, which promotes cooling and condensation of the heavier vapor components before the gas stream proceeds to the filtration stage.

The gas filtration unit represented by item (4) consists of a laboratory-built system composed of layers of hydrophilic cotton and dried milled biomass placed inside a PET bottle. This assembly is used to retain residual condensable droplets and moisture present in the gas stream prior to gas flow measurement and collection. The filtration material is therefore not activated charcoal, and the filtration unit is not a commercial device.

The non-condensable gases (item 5) were collected in flexible gas sampling bags connected to the outlet line after the filtration stage. These bags were used to store the gases for subsequent gas chromatography analysis.

2.3.2. Selection of Operating Temperatures and Heating Rate

The selection of the reactor operating temperatures was guided by the TGA of the tire rubber feedstock. The TGA results indicated an intense thermal degradation region between 400 and 600 °C, corresponding to the main devolatilization and breakdown of the rubber matrix. Based on this behavior, three operating temperatures of 400, 500, and 600 °C were selected to systematically evaluate the influence of temperature on product distribution and energy performance.

The heating rate was chosen considering several criteria, including the maximum operational limit of the reactor (20 °C·min^{-1}), the objective of minimizing electrical energy consumption, the optimization of liquid and gaseous fuel production, and consistency with previous studies employing fixed-bed reactors. Berrueco et al. [27] reported oil yields between 30 and 43 wt.% and gas yields between 2.4 and 4.4 wt.% when operating within a temperature range of 400–700 °C at a heating rate of 15 °C·min^{-1}, which overlaps the conditions investigated in this study. In contrast, the heating rate adopted by Kyari, Cunliffe, and Williams [28] was not considered optimal due to longer residence times and the absence of experiments at 400 and 600 °C.

Additionally, Williams, Besler, and Taylor [29] reported gas yields of approximately 35 wt.% and oil yields of 10 wt.% when applying temperatures between 300 and 720 °C with heating rates ranging from 5 to 80 °C·min^{-1}. Considering these findings, the maximum heating rate supported by the reactor, namely 20 °C·min^{-1}, was selected to enhance process efficiency while remaining consistent with literature benchmarks.

2.3.3. Preliminary Tests and Adjustment of the Effective Reactor Volume

Prior to the main experimental campaign, a series of preliminary tests was performed to verify the operational integrity of the pyrolysis system and identify potential limitations. Leak-tightness was assessed by applying detergent to all system connections while injecting nitrogen at a pressure of 103.421 kPa, equivalent to that used during the experimental runs. The absence of bubbles and audible leaks confirmed the system's airtightness. Furthermore, identical flow readings obtained from two independent rotameters installed at different positions in the system confirmed the absence of leakage.

Fourteen preliminary test runs were subsequently conducted to evaluate the internal behavior of the reactor during pyrolysis. The purpose of running them was to initially understand how the placement of biomass in the reactor could affect the whole experimental run and the results, looking to facilitate experimental tests. It was observed that rubber material positioned within 50 mm of both the lower reactor base and the upper flange became excessively wetted by condensed liquid products, indicating inadequate vapor removal. This behavior was attributed to excessive compaction of the feedstock, which hindered effective gas flow through the bed.

To mitigate this issue, the rubber was redistributed to improve internal gas circulation. However, complete resolution was only achieved after recognizing that the extremities of the reactor were not thermally insulated. Consequently, a perforated aluminum spacer with a diameter of 45 mm and a height of 80 mm was installed at the bottom of the reactor, ensuring that the rubber feedstock remained concentrated in the central, thermally insulated region. Additionally, rubber loading was restricted to avoid the upper 50 mm below the flange. These modifications effectively eliminated liquid accumulation inside the reactor.

As a consequence of these adjustments, the effective reactor height was reduced from 260 mm to 130 mm, resulting in a final useful volume of approximately 401.52 mL, which corresponds to a 50% reduction in the original reactor volume. Accordingly, the feedstock mass per batch was reduced to 100 g to ensure proper operation and reproducibility.

2.3.4. Control and Optimization of N_2 Flow Rate

During the preliminary tests, it was observed that insufficient nitrogen flow rates led to vapor condensation on the internal reactor walls and accumulation of liquid at the reactor bottom. An initial nitrogen flow rate of 1 $L \cdot min^{-1}$ was therefore applied, which successfully displaced all condensable vapors toward the external condenser. Subsequently, the flow rate was progressively reduced in increments of 0.1 $L \cdot min^{-1}$ until reaching the minimum rotameter reading of 0.1 $L \cdot min^{-1}$, which was adopted as the nominal operating flow rate for all experiments.

An additional phenomenon observed was the emergence of a natural vapor-driven gas flow during reactor operation, which increased the total gas flow measured downstream of the gas filter. This flow corresponded to the sum of the nitrogen carrier gas and the pyrolysis-generated gases. As a result, nitrogen injection could be temporarily interrupted when downstream gas flow exceeded 0.2 $L \cdot min^{-1}$ and resumed only when it dropped below the nominal value, significantly reducing nitrogen consumption per batch.

This nominal flow rate is higher than that reported by Zabaniotou and Karabelas [30], who used 0.03 $L \cdot min^{-1}$ of helium, and lower than the 1.5 $L \cdot min^{-1}$ of nitrogen employed by Conesa et al. [31].

Before each experimental run, a nitrogen purge was applied to remove residual air from the reactor. Considering the total reactor volume of 803.04 mL, a pre-experimental purge flow rate of 10 $L \cdot min^{-1}$ was selected, which is 100 times greater than the nominal flow rate. The purge time was calculated using Equation (3), resulting in an injection time of approximately 5 s. All experiments were initiated at a reactor temperature of 35 °C and conducted in quintuplicate to ensure reproducibility, with the reported results expressed as mean values ± standard deviation.

2.3.5. Bubble Condenser and Gas Filtration System

The condensation system consisted of a bubble condenser assembled using a 2 L glass bottle, silicone tubing, and a sealing stopper. Upon exiting the reactor, pyrolysis vapors were forced to bubble upward through water maintained at 26 °C, promoting phase change and efficient condensation of condensable compounds.

The condensed liquid was separated from the water using a 1 L volumetric flask. After decantation, the final liquid volumes were measured using 50 mL and 10 mL graduated cylinders.

Downstream of the condenser, a gas filtration system was installed to remove residual aerosols and moisture. The filter was constructed from a 1 L PET bottle containing three compact layers composed of hydrophilic cotton and milled biomass previously dried at 103–105 °C in a muffle furnace. The cotton layers retained entrained liquid droplets, while the biomass acted as a moisture scavenger.

After approximately 14 test runs, saturation of the upper cotton layer and moisture accumulation in the biomass were observed, requiring replacement of the filter layers every 12 runs to maintain system efficiency. Following filtration and flow measurement, the non-condensable gases were stored in gas sampling bags, which were connected to the system only after the reactor reached the target experimental temperatures of 400, 500, and 600 °C. Product yields were determined by mass balance. The gas yield was calculated by difference from the initial feedstock mass after subtracting the masses of the solid (char) and liquid fractions. Product yields were determined by mass balance. The gas yield was calculated by difference from the initial feedstock mass after subtracting the masses of the solid (char) and liquid fractions.

2.4. Analysis of Gaseous Products

2.4.1. Gas Chromatography

The composition of the non-condensable gases was analyzed using a gas chromatograph (SRI 8610C) equipped with a 5 m × 1/8″ packed column containing a molecular sieve 5A stationary phase, which is suitable for the separation of light gases. Sample injection was performed using a six-port pneumatic valve, ensuring high repeatability and precise control of the injected volume.

The carrier gas flow rate was maintained constant at 20 mL·min^{-1}. Nitrogen (N_2) was used as the carrier gas for hydrogen (H_2) analysis. Meanwhile, hydrogen (H_2) was employed as the carrier gas for methane (CH_4) and carbon monoxide (CO) analyses, in order to optimize chromatographic sensitivity and detector response for each target component.

The chromatographic oven was operated under isothermal conditions at 80 °C, which proved adequate for efficient separation of the analyzed gases. Detection was carried out using a thermal conductivity detector (TCD) maintained at 180 °C, with the operating current set to 165 mA, allowing high sensitivity within the concentration range investigated.

System calibration was performed using a certified standard gas mixture containing H_2, CH_4, and CO with known molar fractions. Quantification of the individual gas components produced during pyrolysis strictly followed the procedures established in ABNT NBR 14903:2014 [32], ensuring metrological traceability and compliance with recognized analytical standards.

2.4.2. Calculation of the HHV and LHV of the Gas

The determination of the calorific value of the non-condensable gases was performed based on their molar composition obtained by gas chromatography. Following the procedures established in ABNT NBR 15213:2008 [33], the molar mass of the gas mixture and the corresponding higher heating value (HHV) and lower heating value (LHV) were calculated as described below.

First, the average molar mass of the mixture was determined as the molar-fraction-weighted sum of the individual molar masses of the constituent species, according to Equation (1):

$$M = x_{H_2} M_{H_2} + x_{CH_4} M_{CH_4} + x_{CO} M_{CO} \quad (1)$$

where M is the molar mass of the mixture (kg·kmol^{-1}), x_i is the molar fraction of component *i*, and M_i is its corresponding molar mass.

The HHV and LHV of the gas mixture were calculated by combining the energetic contribution of each species, weighted by their molar fractions corrected by the ratio between the component molar mass and the total molar mass of the mixture, as expressed in Equation (2):

$$M = x_{H_2}\left(\frac{M_{H_2}}{M}\right) HV_{H_2} + x_{CH_4}\left(\frac{M_{CH_4}}{M}\right) HV_{CH_4} + x_{CO}\left(\frac{M_{CO}}{M}\right) HV_{CO} \quad (2)$$

In this equation, HV represents the heating value of the gas mixture (either HHV or LHV, in MJ·m^{-3}), and HV_i corresponds to the individual heating value (HHV or LHV) of each gas species.

The molar masses and corresponding heating values used in the calculations are presented in Table 1, according to ABNT NBR 15213:2008 [33]. In this table, M_i denotes the molar mass of each gas species $\left(\text{kg·kmol}^{-1}\right)$, while HHV_i and LHV_i represent the higher and lower heating values, respectively, determined at 20 °C and 101.325 kPa $\left(\text{MJ·m}^{-3}\right)$.

Table 1. Thermochemical Properties of the Gases According to ABNT NBR 15213:2008 [33].

Property	H_2	CH_4	CO
M_i $\left(\text{kg}\cdot\text{kmol}^{-1}\right)$	2.0159	16.043	28.010
HHV_i $\left(\text{MJ}\cdot\text{m}^{-3}\right)$	11.889	37.044	11.760
LHV_i $\left(\text{MJ}\cdot\text{m}^{-3}\right)$	10.050	33.367	11.760

These parameters enabled precise quantification of the energetic content of the gaseous fraction formed during pyrolysis, supporting the assessment of thermal efficiency and overall energetic viability of the process.

2.5. Analysis of Liquid Products

After the decantation step, which enabled the complete phase separation between the pyrolytic liquid and the condenser water, the samples were characterized in terms of density, acidity, ash content, and kinematic viscosity at 40 °C. All analyses were performed in accordance with the applicable technical standards, and the corresponding experimental methodologies are described in detail in the subsequent subsections.

2.5.1. Density

The density of the liquid fraction obtained from tire pyrolysis was determined using the direct gravimetric method, which is widely employed for liquid characterization due to its simplicity and reliability [34]. Measurements were performed using a 50 mL graduated cylinder placed on a digital analytical balance with a resolution of 0.0001 g.

For each sample, a known volume of the produced liquid, ranging from 35 to 50 mL, was measured at a controlled temperature of 20 °C. The corresponding mass was recorded simultaneously, ensuring minimal exposure to ambient conditions and reducing potential measurement uncertainties. The density (ρ) was then calculated as the ratio between the measured mass (m) and volume (V), according to Equation (3), following standard procedures reported in the literature [34,35]:

$$\rho = \frac{m}{V} \tag{3}$$

where ρ is the density ($\text{kg}\cdot\text{m}^{-3}$), m is the sample mass (kg), and V is the sample volume (m^3).

This procedure was consistently applied to all liquid samples to ensure the comparability and reproducibility of the results.

2.5.2. Acidity Index

The acid value of the liquid fraction samples was determined in accordance with the procedures described in ASTM D974–12 [36]. Due to the dark coloration of the liquid obtained from the pyrolysis process, a sample mass of 2 g was used, and the titration was carried out using a 0.1 N potassium hydroxide (KOH) solution.

After the titration, the acid value was calculated using Equation (4):

$$\text{Acid value} = \frac{(A - B)\, M\, 56.1}{W} \tag{4}$$

In this equation, the acid value is expressed in milligrams of potassium hydroxide per gram of sample ($\text{mg KOH}\cdot\text{g}^{-1}$), representing the amount of base required to neutralize the acidic compounds present in the liquid fraction. The term A corresponds to the volume of KOH solution consumed during the titration of the liquid sample, measured in milliliters.

In contrast, B represents the volume of KOH solution used in the blank titration, also expressed in milliliters, which is subtracted to correct the method. The variable M refers to the molarity of the KOH solution employed in the titration, expressed in $mol \cdot L^{-1}$. Finally, W denotes the mass of the liquid sample used in the analysis, expressed in grams.

2.5.3. Kinematic Viscosity at 40 °C

The kinematic viscosity of the liquid fraction was measured at 40 °C using a digital viscometer (Tanaka, model AKV-202). The analysis was conducted in accordance with ASTM D445–18 [37], which specifies the standard test method for determining the kinematic viscosity of both transparent and opaque liquids (ASTM, 2018).

2.5.4. Ash Content of the Liquid Fraction

The procedures adopted for determining the ash content followed the principles established in ASTM D3174–02 [38] which describes the standard method for ash analysis in coal and coke samples. In this study, liquid samples with a mass of 1 g were weighed into porcelain crucibles using a digital analytical balance with a resolution of 0.0001 g.

Subsequently, the crucibles were heated in a muffle furnace, reaching 500 °C within 1 h. The heating program recommended for coal analysis was then applied, allowing the samples to reach 750 °C at the end of the second hour. The samples were maintained at this final temperature for an additional 2 h to ensure complete combustion of the organic matter. After the thermal treatment, the crucibles were allowed to cool to ambient temperature, and the remaining ash residue was weighed to determine the ash content of the liquid fraction.

2.6. Energy Assessment of the Process

2.6.1. Energy Yield

The energy conversion efficiency (η) of the products obtained from tire rubber pyrolysis was calculated based on the ratio between the total energy content of the generated products and the energy content of the processed feedstock. This efficiency was determined using Equation (5), which accounts for the contributions of the solid, liquid, and gaseous fractions, following standard thermodynamic approaches reported in the literature [39,40]:

$$\eta = \frac{m_{char} \cdot LHV_{char} + m_{liquid} \cdot LHV_{liquid} + \overline{Q}_{gas} \cdot t_r \cdot LHV_{gas}}{m_{rubber} \cdot LHV_{rubber}} \quad (5)$$

In this equation, η represents the energy conversion efficiency of the pyrolysis process. The term m_{char} corresponds to the mass of the solid char produced, expressed in kilograms, while LHV_{char} denotes its lower heating value, expressed in $MJ \cdot kg^{-1}$. The variable m_{liquid} refers to the mass of the liquid fraction obtained, also expressed in kilograms, and LHV_{liquid} represents the corresponding lower heating value of the liquid fraction.

The contribution of the gaseous products is accounted for by the average gas volumetric flow rate, $\overline{Q}_{gas}$, expressed in $m^3 \cdot min^{-1}$, multiplied by the residence time of the process, t_r, expressed in minutes, and by the lower heating value of the gas, LHV_{gas}, expressed in $MJ \cdot m^{-3}$. The denominator of the equation represents the total energy content of the feedstock, where m_{rubber} corresponds to the mass of tire rubber processed, expressed in kilograms, and LHV_{rubber} denotes the average lower heating value of the rubber.

This formulation enables a comprehensive evaluation of the energetic performance of the pyrolysis process by incorporating all product streams into a single efficiency parameter.

2.6.2. Reactor Electrical Energy Consumption

The electric heating elements, with a total rated power (P) of 3000 W, were not operated continuously throughout the experimental runs, but rather under a pulsed operating regime.

However, for the purpose of simplifying the energy balance calculations, the total electrical energy consumption of the reactor (τ) was estimated by considering the total effective operating time of the heating elements (t).

Accordingly, the energy consumption was calculated using Equation (6):

$$\tau = 3000\ [\mathrm{W}] \cdot t \tag{6}$$

In this equation, τ represents the electrical energy consumption of the reactor, expressed in megajoules (MJ). Meanwhile, t denotes the total operating time of the electrical heating elements, expressed in seconds. This approach provides a reasonable approximation of the electrical energy input to the system, enabling consistent comparison between experimental runs and supporting the overall energy-efficiency analysis of the pyrolysis process.

2.6.3. Process Self-Sustainability

To evaluate whether the energy contained in the produced gaseous fraction was sufficient to render the system energetically self-sustainable, the electrical energy consumption of the reactor heating elements was first determined using Equation (6). Subsequently, the energy available from the non-condensable gases was calculated based on Equation (5), leading to the formulation of Equation (7), following standard thermodynamic approaches reported in the literature [39,40]. This approach enabled a quantitative comparison between the electrical energy input required for reactor operation and the chemical energy recovered in the gaseous stream, allowing assessment of the system's potential for energy self-sufficiency through gas recirculation.

$$\tau_{gas} = \overline{Q}_{gas} \cdot t_r \cdot \mathrm{LHV}_{gas} \tag{7}$$

In this equation, τ_{gas} represents the energy content of the non-condensable gases, expressed in megajoules (MJ). The term $\overline{Q}_{gas}$ corresponds to the average volumetric gas flow rate, expressed in $m^3 \cdot min^{-1}$, while t_r denotes the process residence time, expressed in minutes. The variable LHV_{gas} represents the lower heating value of the gas, expressed in $MJ \cdot m^{-3}$.

By analyzing the ratio between the energy contained in the gas phase (τ_{gas}) and the electrical energy consumed by the reactor (τ), it was possible to determine the fraction of the total energy demand that could be supplied by the energy recovered from the non-condensable gases.

2.7. Distillation of the Liquid Products

The distillation of the liquid products obtained from the pyrolysis process was carried out in accordance with ASTM D86–07 [41], which specifies the standard test method for atmospheric distillation of petroleum-based products at a pressure of 101.325 kPa. The liquid fraction was heated to a final temperature of 215 °C, corresponding to the upper temperature limit for gasoline recovery as defined by the Brazilian National Agency of Petroleum, Natural Gas and Biofuels.

3. Results and Discussion

3.1. Rubber Analyses

Table 2 compares the proximate composition of the waste tire rubber analyzed in this study with data reported in the literature. We reveal substantial variability among studies, primarily associated with differences in tire formulation, mineral fillers, and sampling conditions. In general, waste tires are characterized by a high volatile fraction, typically

exceeding 60%, which mainly consists of natural rubber (NR) and synthetic rubbers such as styrene–butadiene rubber (SBR) and butadiene rubber (BR). These elastomeric components undergo extensive thermal decomposition during pyrolysis, governing the formation of condensable vapors and permanent gases [42,43].

In this context, the material investigated in the present work exhibits an exceptionally high volatile content, reaching 95.28% (wet basis) and 96.40% (dry basis), markedly exceeding the values commonly reported in the literature (55–72%). This distinctive feature indicates a strong propensity toward devolatilization and suggests that, under pyrolytic conditions, the feedstock preferentially favors the generation of liquid and gaseous products rather than solid residues. Such behavior is particularly advantageous for pyrolysis-oriented valorization routes focused on fuels and chemical intermediates.

Conversely, the fixed carbon content obtained in this study is remarkably low (<1%), whereas most reported values range between 20 and 33%. Fixed carbon in waste tires is largely associated with carbon black, which is intentionally incorporated during tire manufacturing to enhance mechanical strength and abrasion resistance [44]. Therefore, the reduced fixed carbon fraction observed here suggests a lower contribution of carbon black in the analyzed rubber. From a process standpoint, this characteristic is expected to limit char formation, simplify downstream solid handling, and shift the product distribution toward the liquid and gaseous fractions.

The ash content measured in this work (≈2.7%) is also significantly lower than those reported in many studies, where ash contents frequently exceed 7% and may reach values above 15%. Ashes originate mainly from inorganic additives such as zinc oxide (ZnO), silica (SiO_2), and other mineral fillers used in tire formulations [45]. Passenger car tires, in particular, tend to exhibit higher ash contents than truck tires due to their greater load of reinforcing inorganic materials [44]. High ash contents can alter thermal degradation pathways, promote catalytic side reactions, and negatively affect pyrolysis oil quality. Accordingly, the relatively low ash content observed in this study constitutes a favorable attribute, as it reduces the likelihood of secondary reactions and contamination of pyrolysis products.

Regarding moisture content, the values obtained (≈1.16–1.17%) are consistent with those commonly reported in the literature. They are sufficiently low to avoid any meaningful impact on the thermal efficiency of the process [46,47]. Moreover, the comparison between wet and dry bases reveals only marginal differences, confirming that the intrinsic compositional characteristics of the rubber dominate its proximate behavior.

Overall, the proximate analysis demonstrates that the waste tire rubber investigated in this study exhibits a distinctive compositional profile, characterized by very high volatility, extremely low fixed carbon, and reduced ash content. These features clearly differentiate it from most waste tire feedstocks reported in the literature and provide a robust basis for interpreting the product yields, energy performance, and physicochemical properties of the fuels obtained in the subsequent sections.

Table 2. Proximate analysis of waste tire rubber reported in the literature and in this study.

Reference	Tire Type	Basis	Volatiles (%)	Moisture (%)	Fixed Carbon (%)	Ash (%)
This work	Waste passenger car tires (mixed brands)	Wet	95.28	1.16	0.85	2.72
		Dry	96.40	1.17	0.86	2.75
[42]	passenger car tires	Wet	63.2	0.2	27.5	9.1
[42]	truck tires	Wet	66.9	0.2	27.8	5.11.5
[48]	Waste tire rubber (WT)	Dry	63.21	–	32.9	3.89
[49]	Waste tire powder	Wet	61.73	0.83	32.59	4.85
[50]	Waste tires (WTs)	Wet	63.1	1.3	26.7	8.9

Table 2. *Cont.*

Reference	Tire Type	Basis	Volatiles (%)	Moisture (%)	Fixed Carbon (%)	Ash (%)
[51]	Mixed waste tire powder	Wet	61.0	1.69	29.62	7.69
[47]	Waste Tire (WT)	Wet	58.59	0.91	24.12	16.38
[52]	Original tire	Wet	62.42	0.97	–	7.51
[53]	Waste tires (Radial)	Dry	72.25	–	19.92	6.87
[43]	Waste tire	Wet	61.0	0.3	25.5	13.2
[44]	Truck ELT rubber	Wet	65.70	0.8	28.10	5.40
[44]	Mix ELT rubber (50:50)	Wet	64.50	0.59	24.89	10.02
[46]	Waste tire (Average)	Wet	55.0	1.5	30.0	13.5

The heating values of waste tire rubber reported in the literature evidence the high energy potential of this solid waste when compared with other biomasses and polymeric residues, as summarized in Table 3. Overall, the (HHV) spans a wide range, from approximately 31 to 45 MJ·kg^{-1}, reflecting variations in rubber composition, carbon black content, elastomer fraction, and inorganic additives.

When compared with conventional solid fuels, waste tires exhibit a markedly superior heating value, exceeding that of coal (≈26–28 MJ·kg^{-1}) and being nearly twice as high as typical woody biomass (≈18–21 MJ·kg^{-1}) [42,54]. The highest HHV values, reported by Khan et al. [55] and reaching up to 45 MJ·kg^{-1}, approach those of liquid fossil fuels, confirming that waste tires constitute a highly energy-dense feedstock well suited for thermochemical conversion routes, particularly pyrolysis.

Differences in heating value are also associated with tire type and formulation. Truck tires and passenger car tires generally exhibit high and relatively similar HHV values (36–38 MJ·kg^{-1}) [42]. However, truck tires tend to present slightly higher values due to their higher natural rubber content and lower inorganic ash fraction [43,56]. Similar HHV values are reported for dry tire rubber samples [48], indicating that chemical composition exerts a stronger influence on energy content than tire typology alone.

Lower HHV values, typically around 32 MJ·kg^{-1}, are reported for mixed tires, tire granules, and end-of-life tires (ELTs) [43,57,58]. These reductions are primarily attributed to higher ash contents and mineral fillers, such as zinc oxide and silica, which do not contribute to combustion and therefore reduce the effective energy density of the material.

Although lower heating value (LHV) data are less frequently reported, they generally range between 30 and 35 MJ·kg^{-1}, depending mainly on moisture content and methodological aspects. As expected, samples with higher moisture levels exhibit lower LHV values [59], emphasizing the relevance of feedstock conditioning for maximizing process energy efficiency. The difference between HHV and LHV further highlights the role of hydrogen content and moisture in tire rubber composition, which are critical parameters for energy balance calculations and thermochemical modeling.

Taken together, the consistently high HHV and LHV values reported in the literature support the classification of waste tires as Tire-Derived Fuel (TDF), explaining their widespread use in cement kilns and thermal power plants [43,54]. Combined with the high volatile contents discussed previously, these characteristics reinforce the potential of waste tires as a strategic feedstock for pyrolysis-based energy recovery, fuel production, and circular economy applications.

Table 3. Heating value of waste tire rubber.

Reference	Sample Type	HHV ($MJ \cdot kg^{-1}$)	LHV ($MJ \cdot kg^{-1}$)
[55]	Waste tire (general)	40.12–45.00	–
[60]	End-of-life tires (ELTs)	38.69	–
[42]	Truck tires (TT)	38.2	–
[42]	Passenger car tires (PCT)	36.5	–
[48]	Tire rubber (dry sample)	36.27	–
[61]	Waste tire (general)	–	35.32
[61]	Tire rubber (simulation)	34.30	32.82
[46]	End-of-life tires (ELTs)	32.95	–
[43]	Tire granules (3, 7, 11 mm)	32.12	–
[57]	Mixed tires (LVT, MVT, HVT)	32.12	–
[58]	End-of-life tires (ELTs)	~32.0	–
[54]	Waste tires (general)	31.4	–
[59]	Waste tire (1.3% moisture sample)	–	30.28

3.2. Fuels Obtained from the Pyrolysis Process

The solid, liquid, and gaseous fuels produced from waste tire rubber pyrolysis were systematically evaluated. The characterization and discussion of these products are presented in Sections 3.2.1–3.2.3, addressing their yields, energetic properties, and physicochemical characteristics.

In order to facilitate a clearer comparison of the effects of temperature on the properties of the products obtained from the pyrolysis process, the main experimental results are summarized in Table 4. The table presents the operating conditions and the key physicochemical and energetic properties of the gaseous, liquid, and solid fractions obtained at the three investigated temperatures (400, 500, and 600 °C). This summary enables direct comparison of variations in gas composition, calorific values, and physicochemical characteristics of the char and liquid products as a function of the final pyrolysis temperature, providing an integrated overview of the influence of temperature on the overall performance of the process.

Table 4. Summary of the main experimental results obtained at different pyrolysis temperatures (400, 500, and 600 °C).

Parameter	Unit	400 °C	500 °C	600 °C
Operating conditions				
Residence time	min	40	25	10
Gas products				
H_2	%	3.06 ± 0.48	7.12 ± 0.87	7.97 ± 0.97
CH_4	%	4.13 ± 0.72	7.93 ± 0.74	10.14 ± 1.22
CO	%	0.77 ± 0.23	0.42 ± 0.07	0.24 ± 0.03
HHV (gas)	$MJ \cdot m^{-3}$	29.62 ± 1.14	32.75 ± 0.31	33.92 ± 0.31
LHV (gas)	$MJ \cdot m^{-3}$	26.90 ± 0.71	29.52 ± 0.27	30.54 ± 0.29
Solid products (char)				
HHV	$MJ \cdot kg^{-1}$	29.52 ±1.68	28.88 ± 1.57	28.83 ± 1.54
LHV	$MJ \cdot kg^{-1}$	29.37 ± 1.69	28.71 ± 1.60	28,65 ± 1.60
Liquid products (pyrolysis)				
Ash content	%	0.43 ± 0.03	0.41 ± 0.06	0.43 ± 0.01
Density	$kg \cdot m^{-3}$	721.60 ± 24.08	724.11 ± 22.27	717.02 ± 14.77

Table 4. *Cont.*

Parameter	Unit	400 °C	500 °C	600 °C
Acidity	Mg KOH· g^{-1}	0.51 ± 0.05	0.54 ± 0.01	0.54 ± 0.01
Kinematic viscosity	$mm^2 \cdot s^{-1}$	5.15 ± 0.84	5.68 ± 0.74	6.86 ± 0.70
HHV	MJ· kg^{-1}	39.82 ± 2.32	41.16 ± 1.70	41.02 ± 1.70
LHV	MJ· kg^{-1}	39.67 ± 2.32	41.54 ± 0.43	41.38 ± 0.44

The influence of temperature on the distribution of pyrolysis products is further illustrated in Figure 2, which presents the relative fractions of gas, char, and liquid obtained at the three investigated temperatures. As the temperature increases from 400 to 600 °C, the gas fraction increases gradually from 26.72% to 32.10%. This behavior is associated with the enhanced thermal cracking of heavier hydrocarbons at higher temperatures. In contrast, the char fraction shows a slight decrease, while the liquid fraction exhibits moderate variations within the investigated temperature range. The graphical representation provides a clear visualization of the changes in product distribution and complements the quantitative data summarized in Table 4.

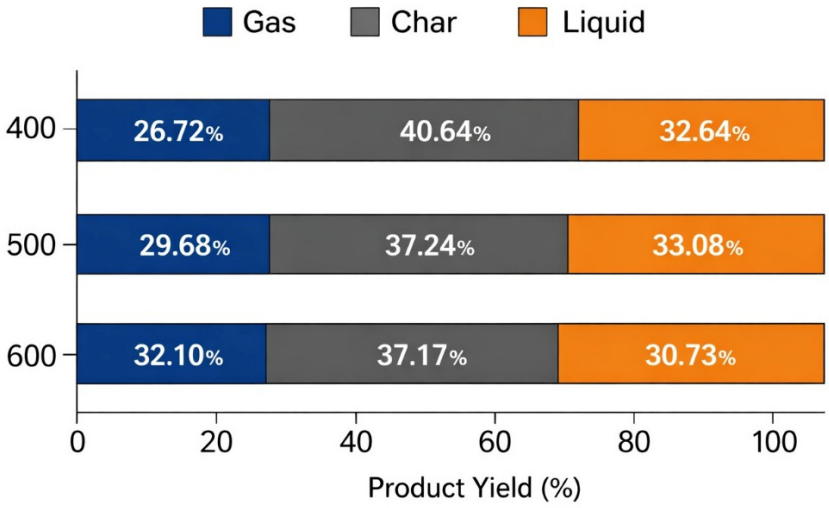

Figure 2. Distribution of pyrolysis products (gas, char, and liquid fractions) obtained at pyrolysis temperatures of 400, 500, and 600 °C.

3.2.1. Gaseous Fraction

The non-condensable gases generated during the pyrolysis of waste tires exhibited a behavior strongly dependent on the operating temperature and the residence time in the reactor, reflecting both the mass yield and the composition and energetic potential of the gaseous fraction. A progressive increase in gas yield was observed with increasing temperature, rising from 26.72% at 400 °C to 29.68% at 500 °C and reaching 32.10% at 600 °C, concomitant with a reduction in residence time from 40 to 10 min. This behavior indicates an intensification of secondary thermal cracking reactions under higher severity conditions, favoring the conversion of condensable vapors and heavy hydrocarbons into lighter gaseous species.

The composition of the gaseous fraction showed a marked increase in hydrogen and methane concentrations with increasing temperature. The H_2 content increased from 3.06% to 7.97%, while CH_4 rose from 4.13% to 10.14% between 400 and 600 °C. In contrast, a continuous decrease in CO concentration was observed, dropping from 0.77% to 0.24% over the same temperature range. This behavior is associated with the higher thermal severity of the process, which promotes thermal reforming, dehydrogenation, and hydrocarbon

chain scission reactions, as well as the conversion of intermediate species into lighter gases through secondary reactions.

The enrichment of the gas in combustible components directly resulted in an increase in its energetic potential. The higher heating value increased from 29.62 $MJ \cdot m^{-3}$ to 33.92 $MJ \cdot m^{-3}$ with increasing temperature, while the lower heating value rose from 26.90 $MJ \cdot m^{-3}$ to 30.54 $MJ \cdot m^{-3}$. These values indicate that the produced gas exhibits a significant energetic potential, compatible with applications such as heat and power generation or integration with other thermochemical processes.

From an operational perspective, the non-condensable gases exhibited a gasoline-like odor, characteristic of the presence of light aromatic and aliphatic hydrocarbons. During the reactor heating stage, maximum gas flow rates ranging from 1.3 to 3.8 $L \cdot min^{-1}$ were recorded. After reaching the operating temperatures, these flow rates stabilized and decreased significantly, reaching approximately 0.1 $L \cdot min^{-1}$ at 400 °C, while at 500 and 600 °C they oscillated between 0.3 and 0.5 $L \cdot min^{-1}$. This behavior reflects a higher intensity of gas generation at elevated temperatures, associated with increased thermal cracking rates.

Knowledge of the gas flow rate at the operating temperatures, combined with the residence time, was fundamental for calculating the total gas volume produced by the reactor and, subsequently, for determining the heating value of the gaseous fraction. It should be noted that gas sampling bags were used exclusively after the system reached the operating temperatures; therefore, the data presented refer only to the conditions of 400, 500, and 600 °C, ensuring greater representativeness and consistency in the analysis of gas composition and energetic performance.

Overall, the results obtained are consistent with trends widely reported in the literature on waste tire pyrolysis. Ramani et al. [56] reported gas yields of approximately 25% at 500 °C, increasing to values above 45% at 750 °C, with extremely short residence times (~4–5 s). These authors also observed substantial increases in H_2 and CH_4 concentrations with increasing temperature, evidencing the intensification of secondary cracking of pyrolysis vapors under rapid heating conditions, which explains the higher gas yields compared to those obtained in this study, conducted under longer residence times.

Similar results were reported by Cepic et al. [43], who observed an increase in gas yield from 16.5% at 500 °C to 33.5% at 750 °C with constant residence times of 90 s, along with a progressive increase in the CH_4 fraction with temperature. These findings reinforce the dominant role of temperature in defining the distribution of gaseous products, regardless of differences in scale, reactor configuration, or heating regime.

The H_2 and CH_4 contents obtained in this study are within the same order of magnitude as those reported by Khan et al. [55], who, operating at 500 °C with a residence time of 60 min, reported gas yields close to 24% and H_2 and CH_4 concentrations of approximately 5% and 11%, respectively. This similarity indicates that, even under prolonged residence times, thermal severity remains the determining factor for the formation of these species, while kinetic aspects influence the extent of secondary reactions.

In contrast, Shao et al. [47] reported a distinct behavior at 600 °C and a residence time of 30 min, with a relatively low gas yield (≈9.3%) but a high CH_4 concentration (≈41%), resulting in a gas with a high lower heating value (~38.8 $MJ \cdot m^{-3}$). This result demonstrates that lower mass yields do not necessarily imply lower energetic quality, as the gas composition may be strongly enriched in light hydrocarbons. By comparison, the gas produced in this study exhibited lower heating values compatible with medium- to high-energy pyrolysis gases, associated with the progressive increase in H_2 and CH_4 with temperature.

Temperature is widely recognized as the main factor influencing gas production and enrichment in light species during waste tire pyrolysis. Increasing temperature promotes secondary cracking of rubber polymers and organic vapors, leading to the conversion of heavy hydrocarbons into H_2 and CH_4 and reducing the fraction of condensable compounds, as discussed by Cepic et al. [43] and Ramani et al. [56]. Additionally, Fan et al. [62] observed that the yields of all gaseous components increased with temperature, with H_2 being the dominant component under high thermal severity conditions, which is consistent with the trends observed in the present study.

Residence time and particle characteristics also exert a relevant influence on gas formation. Longer residence times or larger particles tend to increase gas yield by prolonging exposure to secondary thermal degradation reactions, thereby enhancing further breakdown of polymer chains and pyrolysis vapors, as discussed by Maganinho et al. [58] and Shao et al. [47]. These variables help explain the differences observed among studies conducted at similar temperatures but under distinct heating and residence regimes.

Overall, the results demonstrate that the combination of temperature, residence time, and reactor characteristics plays a decisive role in defining both the yield and the energetic quality of the gaseous fraction, confirming that waste tire pyrolysis gas presents a strong potential as an energy vector and can be optimized according to the intended energy application.

3.2.2. Solid Fraction

The solid fraction obtained during the pyrolysis of waste tires exhibited moderate variation as a function of operating temperature and residence time, directly reflecting the mechanisms of thermal degradation of the polymeric matrix and the extent of secondary reactions. In the present study, the char yield decreased with increasing temperature, from 40.64% at 400 °C to 37.24% at 500 °C and reaching 37.17% at 600 °C, concomitant with a reduction in residence time from 40 to 10 min. This behavior is characteristic of pyrolysis processes in which higher temperatures favor the progressive conversion of the solid fraction into volatile products, particularly liquids and gases, through intensified cracking and devolatilization reactions.

The relatively modest reduction in char yield between 500 and 600 °C indicates that, beyond a certain thermal threshold, the additional degradation rate of the solid phase tends to stabilize. This suggests that most rubber devolatilization occurs within intermediate temperature ranges and is consistent with studies reporting increased thermal stability of the residual carbonaceous structure after the removal of the most reactive volatile components. Ramani et al. [56] reported a similar trend, with char yields of approximately 43.2% at 500 °C decreasing to about 35.2% at 750 °C, even under extremely short residence times. Complementarily, Cepic et al. [43] indicated that above approximately 600 °C, char yield tends to stabilize, as most of the organic matter has already been removed, leaving predominantly the original carbon black and inorganic ash, which is fully consistent with the stability observed between 500 and 600 °C in this study.

Results reported by Fan et al. [62] further reinforce the strong combined influence of temperature and residence time on solid fraction yield. These authors observed high char yields (68.14%) at 450 °C with a residence time of 60 min, whereas at 750 °C under the same residence time, the yield decreased to 41.18%. This comparison demonstrates that longer residence times combined with lower temperatures favor solid retention, while more severe thermal conditions intensify conversion to volatile products, even when thermal exposure is prolonged.

From an energetic standpoint, the produced char exhibited high heating values, with a slight decrease as temperature increased. The higher heating value ranged from

29.52 MJ·kg^{-1} at 400 °C to 28.83 MJ·kg^{-1} at 600 °C, while the lower heating value varied between 29.37 MJ·kg^{-1} and 28.65 MJ·kg^{-1} over the same temperature range. This trend is consistent with the behavior reported by Ramani et al. [56], who observed a decrease in char HHV with increasing pyrolysis temperature up to approximately 600 °C. This phenomenon is associated with the progressive removal of hydrogen from the solid surface during devolatilization, as hydrogen has a high heating value and its depletion negatively affects the energetic content of char [43,56].

After stabilization of devolatilization reactions, the heating value tends to remain approximately constant, predominantly reflecting the energy associated with the remaining elemental carbon. This behavior explains the small variation observed between 500 and 600 °C in this study and is consistent with the results reported by Cepic et al. [43], who found HHV values close to 28.5–29.1 MJ·kg^{-1} for chars produced between 500 and 750 °C. Similarly, Campuzano et al. [60] reported HHV values of approximately 26.6 MJ·kg^{-1} for char produced at 475 °C, highlighting the direct relationship between pyrolysis temperature, solid composition, and energetic performance.

Residence time plays a fundamental role in char formation and quality. In advanced reactors, such as fluidized beds, studies indicate that the time required for complete pyrolysis decreases significantly with increasing temperature, for example, from approximately 55 s at 600 °C to about 34 s at 700 °C [63,64]. Proper synchronization between particle residence time and reactor residence time is essential to avoid energy waste and to ensure efficient rubber conversion, particularly in larger-scale applications [64].

In addition to yield and heating value, the physical and morphological quality of char is strongly influenced by pyrolysis temperature. Chars produced at lower temperatures, such as 400 °C, may exhibit sticky characteristics due to incomplete pyrolysis and the residual presence of partially degraded organic compounds [56,64]. In contrast, higher temperatures promote greater aromatization and reorganization of the carbonaceous structure, improving morphological properties and increasing specific surface area (BET), thereby bringing the recovered char closer to the characteristics of commercial carbon blacks, such as N660 [56].

Overall, the results demonstrate that the solid fraction derived from waste tire pyrolysis exhibits thermochemical behavior fully consistent with the literature and is strongly governed by temperature, residence time, and reactor configuration. The combination of these parameters defines not only char yield, but also its energetic quality and application potential, reinforcing that waste tire pyrolysis char can be directed both to energy applications and to higher value-added uses, such as activation, adsorption, or partial substitution of commercial carbon black, provided that operating conditions are appropriately optimized.

3.2.3. Liquid Fraction

The liquid fraction obtained in this study presented yields ranging from 30.73 to 33.08 wt.%, with the maximum value observed at 500 °C (33.08%), followed by 400 °C (32.64%) and a slight reduction at 600 °C (30.73%). These results are consistent with the range reported by Berrueco et al. [27], who observed liquid yields between 30 and 43 wt.% for temperatures between 400 and 700 °C. The absence of significant variation between 400 and 500 °C suggests that, within this temperature interval, primary depolymerization reactions dominate and favor the formation of condensable hydrocarbons. In contrast, the reduction observed at 600 °C can be attributed to intensified secondary cracking reactions, which promote the formation of lighter, non-condensable gases at the expense of the liquid fraction.

During reactor operation, the condensation process was visually monitored at the water bubbler surface, where two distinct liquid phases were identified. The first phase exhibited a yellowish coloration and partial miscibility with water, indicating the presence of lighter and possibly more polar compounds. As the process progressed, a second, darker phase was formed, characterized by lower density than water, hydrophobic behavior, and a strong odor typical of tire pyrolysis oil. This second fraction displayed higher viscosity, which prevented easy detachment from the glass walls of the collection vessel. At 400 °C, the color of this phase was greenish, while at 500 and 600 °C it shifted to a brown tone, suggesting increased formation of aromatic and heavier hydrocarbon structures at higher temperatures. Only the water-insoluble fraction was considered in the physicochemical analyses, meaning that the reported liquid yield corresponds exclusively to the fuel-like fraction.

The density of the liquid fraction remained relatively stable across the evaluated temperatures, with values of 721.6 $kg \cdot m^{-3}$ at 400 °C, 724.11 $kg \cdot m^{-3}$ at 500 °C, and 717.02 $kg \cdot m^{-3}$ at 600 °C. This limited variation indicates that the overall average molecular weight of the hydrocarbon mixture does not change substantially within the studied temperature range. The obtained values fall within the 700–770 $kg \cdot m^{-3}$ interval, which is comparable to the density range of gasoline (700–800 $kg \cdot m^{-3}$), as reported by Shamsul, Shamsul, Kamarudin, and Rahman [65]. This similarity reinforces the potential applicability of the produced oil in fuel blending or as an alternative hydrocarbon source.

The acidity values were consistently low, ranging from 0.51 to 0.54 mg $KOH \cdot g^{-1}$. At 400 °C, slight oscillations between 0.4 and 0.6 mg $KOH \cdot g^{-1}$ were observed, whereas at 500–600 °C the values stabilized between 0.51 and 0.56 mg $KOH \cdot g^{-1}$. These low acidity levels are significantly lower than those typically reported for lignocellulosic bio-oils, reflecting the hydrocarbon-rich and low-oxygen nature of tire-derived liquids. The limited variation with temperature suggests that the formation of acidic species is not strongly influenced within the 400–600 °C range, contributing to improved fuel stability and reduced corrosive potential.

The kinematic viscosity increased progressively with temperature, from 5.15 $mm^2 \cdot s^{-1}$ at 400 °C to 5.68 $mm^2 \cdot s^{-1}$ at 500 °C and 6.86 $mm^2 \cdot s^{-1}$ at 600 °C. This increase may be associated with enhanced secondary reactions leading to greater formation of aromatic and polyaromatic hydrocarbons. The darker coloration observed at higher temperatures supports this interpretation. Despite the increase, the viscosity values remain within a technically manageable range for energy applications, particularly when considering blending strategies or mild upgrading processes.

Regarding the energetic properties, a gradual increase in heating value was observed with increasing temperature. The higher heating value (HHV) increased from 39.82 $MJ \cdot m^{-3}$ at 400 °C to 41.16 $MJ \cdot m^{-3}$ at 500 °C and 41.54 $MJ \cdot m^{-3}$ at 600 °C, while the lower heating value (LHV) followed the same trend, rising from 39.67 to 41.38 $MJ \cdot m^{-3}$. Although the difference between 500 and 600 °C was not substantial, the liquid produced at 400 °C exhibited slightly lower energy content, indicating that higher temperatures favor the formation of more energy-dense hydrocarbons. These values are in close agreement with those reported by Ucar et al. [66], who determined a HHV of 41.6 $MJ \cdot kg^{-1}$ at 650 °C, and by Rodríguez et al. [67], who reported approximately 42 $MJ \cdot kg^{-1}$ over the 300–700 °C range. The similarity between the present results at 500–600 °C and the literature data confirms the reliability of the obtained liquid fraction and its energetic competitiveness relative to conventional fossil-derived fuels.

Overall, the results indicate that 500 °C represents an optimal operational condition for maximizing liquid yield, while 600 °C slightly enhances energy content at the expense of yield. The produced liquid fraction exhibits low acidity, a stable density within the

gasoline range, moderate viscosity, and a heating value comparable to that of fossil fuels. These characteristics reinforce the suitability of tire pyrolysis oil produced between 500 and 600 °C for energetic applications, particularly as a potential blending component or alternative liquid fuel.

3.2.4. Distilled Fuel

From the liquid fraction obtained by pyrolysis, a distillation process was carried out according to the methodology described in Section 2.7, applying a maximum temperature of 215 °C, similar to the upper limit commonly used for gasoline fractions. The distilled product exhibited a color ranging from yellowish to light brown, indicating the predominance of lighter hydrocarbon fractions compared to the crude pyrolysis oil. This visual change is consistent with the removal of heavier and more aromatic compounds originally present in the whole liquid fraction.

The heating value of the distilled fuel was determined following the same procedure previously adopted for the crude liquid fraction. The results showed high energy content, with higher heating values of 44.14 MJ·m^{-3} at 400 °C, 43.75 MJ·m^{-3} at 500 °C, and 43.30 MJ·m^{-3} at 600 °C. The lower heating value followed a similar trend, decreasing from 43.96 MJ·m^{-3} at 400 °C to 43.57 MJ·m^{-3} at 500 °C and 43.11 MJ·m^{-3} at 600 °C.

A slight reduction in heating value is observed as the pyrolysis temperature increases from 400 to 600 °C. This behavior can be attributed to structural changes in the crude pyrolysis oil produced at higher temperatures. At elevated temperatures, intensified secondary reactions promote the formation of heavier aromatic and polyaromatic compounds. Since the distillation was limited to 215 °C, only the lighter fractions were recovered. Therefore, when pyrolysis is conducted at higher temperatures, a portion of the energy content remains associated with heavier fractions that are not volatilized within the selected distillation range, resulting in a slight decrease in the HHV and LHV of the distilled product.

It is also noteworthy that the LHV values obtained at 500 and 600 °C are very similar, indicating that within this pyrolysis temperature range, the composition of the light fractions recoverable by distillation becomes relatively comparable. This suggests that above 500 °C, further increases in pyrolysis temperature do not significantly modify the energetic characteristics of the light-distilled fuel.

Overall, the HHV values of the distilled fuel (43.30–44.14 MJ·m^{-3}) are higher than those observed for the crude liquid fraction, demonstrating that the distillation process effectively concentrates energy-dense light hydrocarbons. These values are comparable to those of commercial fossil fuels, particularly gasoline, reinforcing the potential of the distilled fraction as a blending component or alternative fuel after appropriate physicochemical adjustments.

The results indicate that pyrolysis at 400 °C, followed by distillation to 215 °C, yields the light fuel fraction with the highest energy content. In contrast, higher pyrolysis temperatures tend to shift part of the energy toward heavier fractions not recovered in this distillation range. Thus, an operational balance between pyrolysis temperature and desired product distribution must be considered depending on the target fuel fraction.

3.2.5. Energy Conversion Yield

Not all the energy contained in the tire rubber feedstock could be recovered at the end of the pyrolysis process due to inherent thermal losses, heat transfer inefficiencies, and energy carried away by non-condensable streams. To quantify the fraction of the rubber's initial energy content transferred to the generated products (liquid, gas, and solid fractions), Equation (5) was used to determine the overall energy conversion yield.

The results indicate that the energy conversion yield increased from 71.1% at 400 °C (40 min residence time) to 74.41% at 500 °C (25 min residence time). However, at 600 °C, when a residence time of only 10 min was applied, the yield decreased significantly to 66.57%. Although the highest LHV of the gaseous fraction was observed at 600 °C, the reduction in overall energy conversion yield at this temperature can be attributed to the short residence time inside the reactor. Due to the limited reaction time, the total volume of gas produced was not sufficient to compensate for process losses and maximize the energy recovered in the product streams.

The short residence time of 10 min at 600 °C was initially selected to prioritize the extraction of the maximum liquid fraction. Nevertheless, even though extending the residence time beyond 10 min does not significantly increase the liquid yield, it may substantially affect the gas production and, consequently, the overall energy recovery.

To investigate this effect, a simulation was performed considering a residence time of 35 min at 600 °C. Under these conditions, the energy conversion yield increased to 74.83%, indicating that longer residence times promote improved conversion of the feedstock energy into recoverable products. This increase suggests that extended exposure to high temperature enhances secondary cracking reactions and gas formation, thereby improving the total energetic recovery of the system.

However, the simulation results must be experimentally validated. It is necessary to determine whether prolonged residence time at 600 °C significantly alters the gas composition, heating value, and volumetric production rate. Additionally, operational aspects must be evaluated, such as whether inert gas injection is required to purge the reactor or whether the gas flow rate remains above 0.1 $L \cdot min^{-1}$, as observed during the 10 min residence time, which is sufficient to ensure continuous gas removal.

Overall, the results demonstrate that energy conversion yield is influenced not only by temperature but also strongly by residence time. While 500 °C provided high and stable energy recovery under experimental conditions, operation at 600 °C requires adequate residence time to fully exploit the energetic potential of the feedstock. Therefore, optimizing both temperature and residence time is essential to maximize the overall energy efficiency of the pyrolysis process.

3.2.6. Reactor Energy Self-Sustainability

One of the main advantages of increasing the volume of gas produced during pyrolysis is the possibility of reinjecting the combustible gas stream into the reactor. Such a strategy may reduce the electrical energy demand required by the heating resistances or, under optimized conditions, potentially render the system energetically self-sustainable.

The ratio between the energy supplied by the gaseous fraction and the electrical energy consumed by the reactor was evaluated to assess this potential. Among the experimentally tested temperatures, the lowest electrical energy consumption was observed at 600 °C, with a total consumption of 7.2 MJ. However, despite this lower energy demand, the highest ratio between gas energy and consumed energy was obtained at 500 °C.

At 400 °C, the average ratio (τ_{gas}/τ) was approximately 1.00 ± 0.03%, indicating that the energy contained in the gaseous fraction was nearly equivalent to the electrical energy consumed during operation, although not sufficient to exceed it. At 500 °C, this ratio increased significantly to 3.28 ± 0.03%, representing the highest value among all evaluated experimental conditions. This result indicates that, at 500 °C, the gaseous fraction has a considerably greater potential to offset the reactor's electrical demand if reinjected into the system. In practical terms, this means that approximately 3.28% of the energy consumed could be supplied by the produced gas under these conditions, making 500 °C the most favorable operational temperature in terms of energetic compensation via gas recirculation.

Although 600 °C required less electrical input, the shorter residence time (10 min) limited the volume of gas produced, resulting in a lower energy compensation ratio (1.70 ± 0.02%). This demonstrates that energy self-sustainability is not solely dependent on reducing electrical consumption but is strongly influenced by the total amount of combustible gas generated and its heating value.

Simulated conditions at 600 °C with extended residence time (35 min) significantly improved this ratio, reaching 3.65 ± 0.04%, which surpasses the experimental result obtained at 500 °C. Under an idealized scenario of infinite residence time, the ratio could theoretically approach 6.79 ± 0.08%, suggesting that prolonged high-temperature operation enhances gas production and, consequently, the energetic recovery potential of the system. Nevertheless, these simulated conditions require experimental validation to confirm their feasibility and to evaluate possible changes in gas composition, heating value, and operational stability.

Overall, the results demonstrate that 500 °C represents the most favorable experimental condition for partial reactor self-sustainability through gas reinjection. In contrast, operation at 600 °C may achieve even higher energetic compensation if adequate residence time is applied. Therefore, optimizing both temperature and residence time is essential to approach an energetically self-sufficient pyrolysis reactor.

4. Conclusions

The results demonstrate that reactor configuration and operational strategy play a decisive role in the pyrolysis performance of waste tire rubber. Proper feedstock arrangement ensuring free gas circulation, combined with an optimized inert gas management strategy, proved essential to avoid vapor condensation inside the reactor, maximize liquid yield, and reduce the consumption of carrier gas.

Temperature strongly influenced product distribution and quality. Increasing the pyrolysis temperature enhanced gas production and improved its energetic quality, with higher H2 and CH4 contents, while reducing CO formation. Although char yield decreased moderately with temperature, its heating value remained high and nearly constant, confirming its potential for energy recovery or further valorization.

Liquid production showed limited sensitivity between 400 and 500 °C, whereas higher temperatures promoted secondary cracking reactions, leading to greater variability in liquid yields. Nevertheless, the pyrolysis oils consistently exhibited high heating values comparable to conventional liquid fuels, along with physicochemical properties compatible with fuel applications, albeit requiring upgrading to meet regulatory specifications.

Energy conversion efficiency was maximized at intermediate temperatures, indicating a favorable trade-off between yield, product quality, and process stability. From an energy perspective, the results highlight the strong potential of waste tire pyrolysis to partially substitute fossil fuels, particularly coal and heavy fuel oil, within the Brazilian energy context.

Overall, this study confirms that waste tire rubber is a highly attractive feedstock for pyrolysis-based energy recovery, offering a technically viable and energetically efficient route for waste valorization, with clear relevance for circular economy strategies and sustainable energy transition.

Author Contributions: H.G.d.L.: Conceptualization, Methodology, Investigation, Formal analysis, Writing—original draft preparation, Data curation; C.M.V.J.: Conceptualization, Supervision, Methodology, Validation, Formal analysis, Writing—review and editing, Funding acquisition; H.S.: Formal analysis, Writing—review and editing, Validation, Project administration; A.F.d.N.J.: Investigation, Experimental setup, Data acquisition, Visualization; A.C.D.A.: Scientific guidance, Validation,

Writing—review and editing; S.P.R.d.S.: Resources, Experimental infrastructure, Methodology support, Supervision. All authors have read and agreed to the published version of the manuscript.

Funding: Clériston Moura Vieira Júnior gratefully acknowledges the financial support provided by the Fundação de Amparo à Ciência e Tecnologia do Estado de Pernambuco (FACEPE), Brazil, under grant numbers IBPG-1224-3.09/20 and BFI-0252-3.01/25. Humberto Santos acknowledges the project PID2023-148958OB-C21, supported by the Ministry of Science, Innovation, and Universities of Spain.

Data Availability Statement: The original contributions presented in this study are included in the article. Further inquiries can be directed to the corresponding author.

Conflicts of Interest: The authors declare no conflicts of interest.

References

1. Dewang, Y.; Sharma, V.; Kumar, Y. A Critical Review of Waste Tire Pyrolysis for Diesel Engines: Technologies, Challenges, and Future Prospects. *Sustain. Mater. Technol.* **2025**, *43*, e01291. [CrossRef]
2. Nuramirah, S.; Muhammad, R.; Fatahah, N.; Zainal, A.; Chay, C. Global Trends of Waste Tire Pyrolysis Research: A Bibliometric Analysis. *Clean. Energy Syst.* **2025**, *10*, 100181. [CrossRef]
3. Alzahrani, N.; Nahil, M.A.; Williams, P.T. Co-Pyrolysis of Waste Plastics and Tires: Influence of Interaction on Product Oil and Gas Composition. *J. Energy Inst.* **2025**, *118*, 101908. [CrossRef]
4. Qi, J.; Wang, Y.; Xu, P.; Hu, M.; Huhe, T.; Ling, X.; Yuan, H.; Li, J.; Chen, Y. Coupling of Molten Salt Heating Tire Pyrolysis Process with Carbon Black Modification Process: Technical Economic Evaluation and Life Cycle Assessment. *J. Clean. Prod.* **2025**, *486*, 144454. [CrossRef]
5. Ma, H.; Bai, Y.; Ma, S. Heat Transfer Performance and Influencing Factors of Waste Tires During Pyrolysis in a Horizontal Rotary Furnace. *Energies* **2025**, *18*, 4028. [CrossRef]
6. Wang, W.; Zhong, Z.; Zheng, X.; Ye, Q.; Li, Y.; Yang, Y. Catalytic Co-Pyrolysis of Hydrolyzed Lignin and Waste Tires over NiMo Modified HZSM-5/MCM-41 Composite Molecular Sieve in Microwave Fluidized Bed for Monocyclic Aromatic Hydrocarbons. *Energy* **2025**, *329*, 136812. [CrossRef]
7. Poblete, J.; Jim, R.; Ronsse, F.; Ghysels, S.; Arteaga-p, L.E. Understanding Limonene Synthesis from Waste Tire Pyrolysis through a Kinetics-Based Perspective. *J. Anal. Appl. Pyrolysis* **2025**, *191*, 107207. [CrossRef]
8. Pšenička, M.; Roudov, A. Pyrolysis Oils from Used Tires and Plastic Waste: A Comparison of a Co-Processing with Atmospheric Gas Oil. *Energies* **2022**, *20*, 7745. [CrossRef]
9. Chybowski, L.; Szczepanek, M.; Pusty, T.; Bro, P.; Pełech, R. Evaluation of the Ignition Properties of Fuels Based on Oil Diesel Fuel with the Addition of Pyrolytic Oil from Tires. *Energies* **2025**, *18*, 860. [CrossRef]
10. Chybowski, L.; Szczepanek, M.; Pusty, T. Rheological Properties of Diesel-Based Fuels with Tyre Pyrolysis Oil as Admixture. *Energies* **2025**, *18*, 1993. [CrossRef]
11. Jaworski, A.; Kuszewski, H.; Szpica, D.; Wo, P.; Balawender, K.; Krzemi, A. Comparative Study on the Effects of Diesel Fuel, Hydrotreated Vegetable Oil, and Its Blends with Pyrolytic Oils on Pollutant Emissions and Fuel Consumption of a Diesel Engine Under WLTC Dynamic Test Conditions. *Energies* **2025**, *18*, 5038. [CrossRef]
12. Guo, S.; Gu, M.; Zhang, X.; Chen, J.; Yao, H. Generation and Utilization of Waste Tires Pyrolysis Carbon: A Critical Review. *Fuel* **2025**, *400*, 135740. [CrossRef]
13. Yakut, R.; Erkmen, J.; Gümüs, M. Effect of Using Waste Ash Resulting from Tire Pyrolysis in Hydrophobic Geopolymer Production on Thermal Insulation, Sound Insulation and Waterproofing. *Therm. Sci. Eng. Prog.* **2025**, *62*, 103646. [CrossRef]
14. Zhao, S.; Wen, X.; Tang, D.; Xu, Y.; Sun, C.; Zhao, H.; Pei, X.; Lin, L. Improved Wear Resistance of Natural Rubber-Based Tire Materials via Constructing Carbon Black/Ar Plasma Modified Pyrolysis Carbon Black Hybrid Filler Network. *Tribol. Int.* **2025**, 111111. [CrossRef]
15. Caspani, S.; Manenti, F. Hydrogen Recovery from End-of-Life Tire Pyrolysis Gas via H2S Splitting. *Int. J. Hydrogen Energy* **2025**, *144*, 1292–1298. [CrossRef]
16. Messerle, V.; Ustimenko, A. Plasma Processing of Rubber Powder from End-of-Life Tires: Numerical Analysis and Experiment. *Processes* **2024**, *12*, 994. [CrossRef]
17. Xu, F.; Shao, Y.; Zhang, Y.; Zong, P. Parametric Investigation of the Effects on Waste Tire Pyrolysis Oil in a Downdraft Tube Reactor. *Energy* **2025**, *314*, 134267. [CrossRef]
18. Arteaga-Pérez, L.E.; Larrere, S.; Chávez-Delgado, M.; Ordoñez, Y.J.R.; Concha, J.L.; Segura, C.; Norambuena-Contreras, J.; Casas-Ledón, Y. Environmental Life Cycle Assessment of Encapsulated Rejuvenators from Mining Truck Waste Tires via Pyrolysis for Asphalt Self-Healing. *J. Clean. Prod.* **2025**, *490*, 144787. [CrossRef]

19. Li, G.; Zhang, X.; Wang, S.; Zhang, J.; Yang, H.; Zeng, K.; Shao, J.; Zhang, S.; Chen, H. Migration and Transformation of Sulfur during Pyrolysis of Waste Tires for High-Value Utilization of Poly-Generation Products. *Waste Manag.* **2025**, *203*, 114868. [CrossRef]
20. Xu, Q.; Chen, Z.; Xian, S.; Li, H.; Wu, Y. In-Situ Sulfur Fixation Mechanism during Microwave Fluidized-Bed Co-Pyrolysis of Waste Tires and Biomass. *J. Clean. Prod.* **2025**, *494*, 145030. [CrossRef]
21. Thornton, S.A.; Milton, S.G.; Lautermilch, L.R.; Massarsky, A.; Unice, K.M. Pyrolysis-GC/MS Calibration for Environmental Quantification of Tire Tread: Standards and Marketplace Averaged Elastomer Subunit Profiles. *Chemosphere* **2025**, *385*, 144554. [CrossRef] [PubMed]
22. Xu, Y.; Fu, S.; Wen, Y.; Lv, W.; Ma, L.; Hu, H.; Jin, L. Synthesis of α-Terpinyl Methyl Ether by Catalytic Alkoxylation of Tire Pyrolysis Oil over Heteropolyacid Modified Hβ Zeolite. *Chem. Eng. Sci.* **2025**, *311*, 121572. [CrossRef]
23. Sanchís, A.; Navarro, M.V.; Veses, A.; Martínez, J.D.; Call, M.S.; Manuel, L. Pyrolysis of Different Types and Sections of End-of-Life Tyres: Kinetics and Experiments to Improve Product Quality. *J. Anal. Appl. Pyrolysis* **2025**, *192*, 107309. [CrossRef]
24. *ASTM D3172*; Standard Practice for Proximate Analysis of Coal and Coke. ASTM International: West Conshohocken, PA, USA, 1989.
25. *ABNT NBR 8633*; Carvão Vegetal: Determinação do Poder Calorífico: Método de Ensaio. Associação Brasileira de Normas Técnicas: Rio de Janeiro, Brazil, 1984.
26. Silva, L.L.O. *Desenvolvimento de Um Reator Em Batelada Para Pirólise de Resíduos Plásticos*; University of Pernamuco: Recife, Brazil, 2017.
27. Berrueco, C.; Esperanza, E.; Mastral, F.J.; Ceamanos, J.; Garcı, P. Pyrolysis of Waste Tyres in an Atmospheric Static-Bed Batch Reactor: Analysis of the Gases Obtained. *J. Anal. Appl. Pyrolysis* **2005**, *74*, 245–253. [CrossRef]
28. Kyari, M.; Cunliffe, A.; Williams, P.T. Characterization of Oils, Gases, and Char in Relation to the Pyrolysis of Different Brands of Scrap Automotive Tires. *Energy Fuels* **2005**, *19*, 1165–1173. [CrossRef]
29. Williams, P.T.; Besler, S.; Taylor, D.T. The Pyrolysis of Scrap Automotive Tyres. The Influence of Temperature and Heating Rate on Product Composition. *Fuel* **1990**, *69*, 1474–1482. [CrossRef]
30. Zabaniotou, A.; Karabelas, A.J. Pyrolysis as a Method for Utilization of Solid Wastes in Greece (Agricultural Wastes and Used Tyres). In *Progress in Thermochemical Biomass Conversion*; Bridgwater, A.V., Ed.; CPL Press: Newbury, UK, 2003.
31. Conesa, J.A.; Martín-Gullón, I.; Font, R.; Jauhiainen, J. Complete Study of the Pyrolysis and Gasification of Scrap Tires in a Pilot Plant Reactor. *Environ. Sci. Technol.* **2004**, *38*, 3189–3194. [CrossRef]
32. *ABNT NBR 14903*; Gás Natural: Determinação da Composição Química por Cromatografia em Fase Gasosa. Associação Brasileira de Normas Técnicas: Rio de Janeiro, Brazil, 2014.
33. *ABNT NBR 15213*; Gás Natural: Cálculo de Propriedades Físico-Químicas a Partir da Composição. Associação Brasileira de Normas Técnicas: Rio de Janeiro, Brazil, 2008.
34. de Jesus, V.L.B.; Palma, D.A. Medição Da Densidade Do Óleo: Uma Discussão Sobre Sua Otimização e Diminuição Dos Custos via Incerteza Relativa Da Medição. *Rev. Bras. Ensino Física* **2008**, *30*, 3302. [CrossRef]
35. Fox, R.W.; McDonald, A.T.; Pritchard, P.J.; Mitchell, J.W. *Introduction to Fluid Mechanics*, 10th ed.; Wiley: Hoboken, NJ, USA, 2020.
36. *ASTM D974*; Standard Test Method for Acid and Base Number by Color-Indicator Titration. ASTM International: West Conshohocken, PA, USA, 2012.
37. *ASTM D445*; Standard Test Method for Kinematic Viscosity of Transparent and Opaque Liquids (and Calculation of Dynamic Viscosity). ASTM International: West Conshohocken, PA, USA, 2018.
38. *ASTM D3174*; Standard Test Method for Ash in the Analysis Sample of Coal and Coke. ASTM International: West Conshohocken, PA, USA, 2002.
39. Borgnakke, C.; Sonntag, R.E. *Fundamentals of Thermodynamics*, 10th ed.; John Wiley & Sons: Hoboken, NJ, USA, 2020.
40. Moran, M.J.; Shapiro, H.N.; Boettner, D.D.; Bailey, M.B. *Fundamentals of Engineering Thermodynamics*, 9th ed.; John Wiley & Sons: Hoboken, NJ, USA, 2020.
41. *ASTM D86*; Standard Test Method for Distillation of Petroleum Products at Atmospheric Pressure. ASTM International: West Conshohocken, PA, USA, 2007.
42. Ramani, B.; Anjum, A.; Bramer, E.; Dierkes, W.; Blume, A.; Brem, G. Flash Pyrolysis of Waste Tires in an Entrained Flow Reactor—An Experimental Study. *Polymers* **2024**, *16*, 1746. [CrossRef]
43. Cepic, Z.; Mihajlovic, V.; Đuric, S.; Milotic, M.; Stošic, M.; Stepanov, B.; Micunovic, M. Experimental Analysis of Temperature Influence on Waste Tire Pyrolysis. *Energies* **2021**, *14*, 5403. [CrossRef]
44. Martín, M.T.; Aguirre, J.L.; Baena-gonz, J.; González, S.; Pérez-Aparicio, R.; Saiz-Rodríguez, L. Influence of Specific Power on the Solid and Liquid Products Obtained in the Microwave-Assisted Pyrolysis of End-of-Life Tires. *Energies* **2022**, *15*, 2128. [CrossRef]
45. Lan, Y.; Jin, S.; Wang, J.; Wang, X.; Zhang, R.; Ling, L.; Jin, M. Effects of S and Mineral Elements (Ca, Al, Si and Fe) on Thermochemical Behaviors of Zn during Co-Pyrolysis of Coal and Waste Tire: A Combined Experimental and Thermodynamic Simulation Study Yaxin. *Processes* **2022**, *10*, 1635. [CrossRef]

46. Hu, Y.; Zhou, J.; Qian, Q.; Ren, J. Innovative Valorization of Waste Tire by Integrating Pyrolysis with Steam Rankine Cycle, Multi-Generation, and Desalination: Novel Process Design, Simulation and Comprehensive Analysis. *Energy* **2025**, *323*, 135812. [CrossRef]
47. Shao, J.; Tian, X.; Fan, T.; Zhang, J.; Wang, S.; Cheng, W.; Zhang, X.; Yang, H.; Zhang, S.; Chen, H. Study on Waste Tires Pyrolysis Characteristics and High-Value Oil: Effects of Pyrolysis Parameters and Catalyst. *J. Energy Inst.* **2025**, *118*, 101934. [CrossRef]
48. Ji, X.; Liu, H.; Chen, J.; Zhou, X.; Li, J.; Yang, L.; Lin, W.; Chen, N. An Experimental Study into the Pyrolysis Characteristics of Waste Tire Rubber with Catalyst Addition. *Chin. J. Chem. Eng.* **2025**, *81*, 128–141. [CrossRef]
49. Wang, B.; Song, Y.; Wang, F.; Fan, Y.; Cheng, N.; Duan, P. Comparative Study on Properties of Waste Tyre Pyrolysis Oil and Its Distillates Obtained by Molecular Distillation. *J. Anal. Appl. Pyrolysis* **2025**, *188*, 107046. [CrossRef]
50. Li, Y.; Shan, T.; Wang, W.; Liu, Y.; Yin, F. Critical Temperature Pyrolysis of Waste Tires: Process Energy Consumption and Product Characteristics. *J. Anal. Appl. Pyrolysis* **2025**, *192*, 107317. [CrossRef]
51. Ye, W.; Xu, X.; Zhan, M.; Huang, Q.; Li, X.; Jiao, W.; Yin, Y. Formation Behavior of PAHs during Pyrolysis of Waste Tires. *J. Hazard. Mater.* **2022**, *435*, 128997. [CrossRef]
52. Abdallah, R.; Juaidi, A.; Assad, M.; Salameh, T.; Manzano-agugliaro, F. Energy Recovery from Waste Tires Using Pyrolysis: Palestine as Case of Study. *Energies* **2020**, *13*, 1817. [CrossRef]
53. Holubcík, M.; Klacková, I.; Durcanský, P. Pyrolysis Conversion of Polymer Wastes to Noble Fuels in Conditions of the Slovak Republic. *Energies* **2020**, *13*, 4849. [CrossRef]
54. Niesler, M.; Stecko, J.; Gierad, D.; Nowak, M.; Stelmach, S. Experimental Production of Iron-Bearing Sinters Using Chars from Waste Car Tires. *Processes* **2023**, *11*, 231. [CrossRef]
55. Khan, A.; Iqbal, N.; Noor, T.; Iqtidar, A.; Khan, N. Pyrolysis of Lignite Coal and Waste Tires for Liquid Fuel Production. *J. Energy Inst.* **2025**, *120*, 102065. [CrossRef]
56. Ramani, B.; Anjum, A.; Bramer, E.; Dierkes, W.; Blume, A. A Comprehensive Study on the Effect of the Pyrolysis Temperature on the Products of the Flash Pyrolysis of Waste Tires. *J. Environ. Chem. Eng.* **2025**, *13*, 115468. [CrossRef]
57. Zerin, N.H.; Rasul, M.G.; Jahirul, M.I.; Sayem, A.S.M.; Haque, R. X Physicochemical Properties of Pyrolytic Char and Oil from Mixed Tyre Using Batch Pyrolysis Process. *Energy Convers. Manag. X* **2025**, *26*, 100941. [CrossRef]
58. Maganinho, C.; Silva, C.M.C.; Costa, M.R.; Mendes, A.; Rocha, J.; Silva, M. Advances in the Pyrolysis of End-of-Life Tires: A Critical Review of Reactor Systems, Process Conditions and Industrial Applications. *J. Environ. Chem. Eng.* **2025**, *13*, 118667. [CrossRef]
59. Xin, C.; Liu, J.; Chen, T.; Chen, H.; Huo, H.; Wang, S.; Wang, Y. Technical and Economic Analysis of a Novel Integrated Energy System with Waste Tire Pyrolysis and Biogas. *Processes* **2025**, *13*, 415. [CrossRef]
60. Campuzano, F.; Agudelo, F.; Daniel, J.; Roberts, W.L. On the Exergoeconomics of the Thermochemical Recycling of End-of-Life Tires by Pyrolysis. *Energy* **2025**, *330*, 136930. [CrossRef]
61. Gui, F.; Chen, H.; Zheng, Q.; Zhao, H.; Pan, P.; Bian, J. Performance Analysis of a Novel Multi-Production Design via the Integration of Medical Waste Plasma Gasification and Waste Tire Pyrolysis. *Energy* **2024**, *313*, 134024. [CrossRef]
62. Fan, D.; Zhang, C.; Liu, C.; Yu, M.; Yao, B.; Chao, L. Pyrolysis of Waste Tires in Fluidized Bed Reactor: Pyrolysis Characteristics and Hazardous Elements Transformation. *Energy* **2025**, *330*, 136801. [CrossRef]
63. Dai, J.; Feng, H.; Oboirien, B.; Liu, S.; Zhang, X.; Wu, Z.; Chen, Z.; Gao, S. Catalytic Upgrading of Waste Tire Pyrolysis Volatiles over Ga/ZSM-5 Catalysts. *J. Anal. Appl. Pyrolysis* **2025**, *192*, 107291. [CrossRef]
64. Chen, Y.; Li, C.; Zhang, Q.; Qu, Y.; Duan, J.; Wang, W. Simulation of Waste Tire Pyrolysis in a Multi-Chamber Fluidized Bed by Coupling CFD-DEM with a Particle Shrinkage Model. *Energy* **2025**, *329*, 136821. [CrossRef]
65. Shamsul, N.S.; Kamarudin, S.K.; Rahman, N.A. Conversion of Bio-Oil to Bio Gasoline via Pyrolysis and Hydrothermal: A Review. *Renew. Sustain. Energy Rev.* **2020**, *80*, 538–549. [CrossRef]
66. Ucar, S.; Karagoz, S.; Ozkan, A.R.; Yanik, J. Evaluation of Two Different Scrap Tires as Hydrocarbon Source by Pyrolysis. *Fuel* **2005**, *84*, 1884–1892. [CrossRef]
67. Rodriguez, I.D.M.; Laresgoiti, M.F.; Cabrero, M.A.; Torres, A.; Chomon, M.J.; Caballero, B. Pyrolysis of Scrap Tyres. *Fuel Process. Technol.* **2001**, *72*, 9–22. [CrossRef]